Available online at www.sciencedirect.com
SCIENCE DIRECT
Polymer 47 (2006) 652–662
polymer
www.elsevier.com/locate/polymer

Delamination of organo-modified layered double hydroxides in polyamide 6 by melt processing

Mauro Zammarano [a,1,*], Séverine Bellayer [a,2], Jeffrey W. Gilman [a], Massimiliano Franceschi [b], Frederick L. Beyer [c], Richard H. Harris [a], Sergio Meriani [d]

[a] *Building and Fire Research Laboratory, National Institute of Standards and Technology, 100 Bureau Drive, Gaithersburg, MD 20899-8665, USA*
[b] *Cimteclab, Area Science Park, Padriciano, 99-34012 Trieste, Italy*
[c] *US Army Research Laboratory, Materials Division, Aberdeen Proving Ground, MD 21005, USA*
[d] *Department of Materials Natural Resources, University of Trieste, Valerio 2, 34127 Trieste, Italy*

Received 7 June 2005; received in revised form 26 November 2005; accepted 28 November 2005
Available online 20 December 2005

Abstract

Layered double hydroxides (LDH) are a class of readily synthesizable layered crystals that can be used as an alternative to the commonly used silicate crystals for the preparation of polymeric nanocomposites. In this work layered double hydroxide/polyamide 6 nanocomposites (LDH/PA6) were prepared from organo-modified LDH by melt processing. The anionic exchange capacity of LDH was varied in order to investigate its influence on the degree of exfoliation. LDH were dispersed by a twin screw micro-extruder at a variety of processing conditions. The nanocomposites were characterized by wide-angle X-ray diffraction (WAXD), small-angle X-ray scattering (SAXS), transmission electron microscopy, dynamic scanning calorimetry, and thermogravimetric analysis. It was found that exfoliated nanocomposites were successfully prepared by melt processing with a low exchange capacity LDH, whereas residue tactoids were observed with a high exchange capacity LDH. Shear, together with the exchange capacity, seems to be the key factor for the delamination in LDH/PA6. No major change in the crystalline phase or in the rate of crystallization was observed in the nanocomposite as compared to the neat polymer. A reduction in the onset of thermal decomposition temperature was observed in PA6/LDH compared to neat PA6, likely due to a nucleophilic attack mechanism. The properties of this nanocomposite system are discussed with connections to the current understanding within the broader nanocomposite field.

Keywords: PA6; Nanocomposite; LDH

1. Introduction

Composite materials reinforced on a molecular scale, so-called nanocomposites, exhibit improved physical and performance properties in comparison to pristine polymers and conventional composites with the addition of only a few percent of the nano-filler [1,2]. Improved tensile and thermal properties [3,4], reduced permeability [5], reduced solvent uptake [6], increased heat distortion temperature [7], and lower flammability [8] have been reported in literature. These improvements are mainly a consequence of the unique interfacial effects that result from the dispersion of the high aspect ratio nanoparticles [9–13]. A mass fraction of a few percent of reinforcing agent that is properly distributed in the polymer matrix creates significantly more surface area for polymer–filler interactions than do conventional composites [14]. Silicate clays such as montmorillonite, hectorite and magadiite are the most common fillers used for the preparation of nanocomposites; they have a layered structure with 1 nm thickness and extremely high aspect ratios (e.g. 50–1000). Lately, a new emerging class of nanocomposites, based on layered double hydroxides (LDH), also known as anionic or hydrotalcite-like clays, has been investigated [15]. LDH have a layered structure with aspect ratios similar to, or even higher, than the ones observed for aluminosilicate clays. LDH layers are 0.48–0.49 nm thick [16,17] and their planar dimensions can be tuned between 60 nm [18] and 20 μm [19] by properly adjusting the synthesis conditions. Anionic clays can be considered as the opposite of silicate clays: positively charged

* Corresponding author. Tel.: +39 6452215283; fax: +39 8318331185.
E-mail address: zammarano@gmail.com (M. Zammarano).
[1] NIST Guest Researcher from CimtecLab, Area Science Park, Padriciano 99-34012 Trieste, Italy.
[2] NIST Guest Researcher from Laboratory GEMTEX of Ecole Nationale Supérieure des Arts et Industries Textiles (ENSAIT).

0032-3861/$ - see front matter © 2005 Elsevier Ltd. All rights reserved.
doi:10.1016/j.polymer.2005.11.080

sheets are stacked one on top of the other and intercalated by exchangeable anions and water molecules [20]. LDH layers consist of edge-sharing octahedral units where each octahedron is formed by a cation coordinated with six hydroxyl groups.

Important features of LDH are the highly tunable intra-layer and inter-layer composition that allow one to fit the properties of the clay to applications in a large number of fields: catalysis and their supports [20], adsorbents [21], ceramic precursors [22], electrochemical reactions [23], stabilizers [24] and gene therapy [25].

The general formula to describe the chemical composition for an octahedral unit is:

$$[M_{1-x}M^{III}_x(OH)_2]^q \qquad [A^{n-}_{q/n}\cdot mH_2O]$$

intralayer composition interlayer composition

where $M=M^{2+}$, divalent cation (Mg^{2+}, Zn^{2+}, Ca^{2+}, Co^{2+}, Ni^{2+}, Cu^{2+}, Mn^{2+}), or $M=M^{+}$ monovalent cation (Li^{+})[3]; M^{3+} = trivalent cation (Al^{3+}, Cr^{3+}, Fe^{3+}, Co^{3+}, Ga^{3+}, Mn^{3+}); A^{n-} = exchangeable interlayer anion; q is the value of layer charge for octahedral unit, $q=x$ for M bivalent cation and $q=2x-1$ for M monovalent cation.

The anionic exchange capacity (AEC) of LDH can be expressed as: $AEC=q/M_w\times10^5$ [mequiv/100 g] where M_w is the weight of the chemical formula for each octahedral unit.

The layer charge q and therefore the AEC can be tuned adjusting the ratio $\rho=(1-x)/x$ between the monovalent/divalent cation M and the trivalent one M^{III}.

Typically LDH exchange capacities vary in the range 200 mequiv/100–470 mequiv/100 g and are higher than the corresponding cation exchange capacity (CEC) of silicate clays like sodium montmorillonite (exchange capacity = 80–145 mequiv/100 g [1,26]). The electrostatic stacking forces between layers and intercalated anions increase with the exchange capacity; this is unfavourable for the exfoliation process [26–28] and may explain the relatively low number of LDH-based nanocomposites reported in literature. Usually only intercalated structures with low *d*-spacings are obtained, as found for poly(styrene sulfonate), poly(vinyl sulfonate), poly(acrylic acid), poly(ethylene oxide) and dioctyl sulphosuccinate LDH nanocomposites [29–32]. Hsueh et al. [33] have claimed a complete exfoliation in polyimide of an aminobenzoate modified LDH by in situ polymerization: an increase of the tensile strength at break and glass transition temperature, and a decrease in the coefficient of thermal expansion is reported for the nanocomposite compared to the neat polymer. Furthermore, the thermal stability was enhanced as dynamic and isothermal thermogravimetric data revealed. Similar results are reported for LDH/epoxy, LDH–acrylate, and LDH–methacrylate nanocomposites by in situ polymerization [34–36]. Intercalated or delaminated structure were also obtained with poly(ethylene oxide) and poly(ethylene)-*graft*-maleic anhydride by solution intercalation [37,38].

In this study, the fabrication and properties of LDH nanocomposites based on polyamide 6 were studied, and the ability to fabricate exfoliated nanocomposites using melt compounding was investigated. It is worthy to note that even if other thermoplastic nanocomposites based on LDH were reported they were obtained by different techniques such as solution intercalation [38] or in situ polymerization [34]. Melt compounding is the most important and widely used approach for the preparation of commercial polymers, and it allows the direct formation of the nanocomposite during extrusion, without using solvents. However, complete exfoliation is usually more difficult to achieve by melt compounding when compared to other techniques. Furthermore, the available literature suggests that LDH exfoliation is hard to achieve compared to phyllosilicates due to the high electrostatic stacking forces between layers and intercalated anions. In this study appropriate LDH with relatively low AEC and high thermal stability have been synthesized. Organic modified Zn–Cr LDH with low AEC were previously reported [39] but their thermal stability was not suitable for melt processing. Furthermore heavy metal compounds such as Cr based LDH cannot be used due to their potential toxicity and poor environmental acceptability. It is particularly true for flame retardant applications where environmental issues are very critical. This is the main potential use for LDH based nanocomposites, which show improved flame retardant properties compared to silicate clays [40]. Mg–Al LDH are environmentally friendly flame retardants and the thermal stability is suitable for our purposes.

2. Experimental[4]

2.1. Materials and synthesis of the organo-modified LDH

Reagent grade metal chlorides $MgCl_2\cdot6H_2O$ (99.6%)[5] and $AlCl_3\cdot6H_2O$ (99%) were obtained from Merck and Aldrich, respectively. A 70% mass fraction of 4-dodecylbenzenesulfonic acid in propanol purchased from Aldrich was used as anionic surfactant after neutralization with sodium hydroxide in an argon atmosphere. The distilled water was further purified using a Barnstead Nanopure II system and held at 60 °C overnight at low pressure in order to minimize CO_3^{2-} in solution. The polyamide 6 (1015 B) was supplied by UBE Chemicals.

[3] The Li–Al LDH is the only known example of a M^{+}–M^{3+} LDH. Li–Al LDH structure is obtained by insertion of Li^{+} ions in the octahedral vacancies of gibbsite (γ-Al(OH)3).

[4] This work was carried out by the National Institute of Standards and Technology (NIST), an agency of the US government, and by statute is not subject to copyright in the United States. Certain commercial equipment, instruments, materials, services, or companies are identified in this paper in order to specify adequately the experimental procedure. This in no way implies endorsement or recommendation by NIST. The policy of NIST is to use metric units of measurement in all its publications, and to provide statements of uncertainty for all original measurements. In this document however, data from organizations outside NIST are shown, which may include measurements in non-metric units or measurements without uncertainty statements.

[5] % (or %w) is used throughout this manuscript and is identical to mass fraction %.

Magnesium–aluminium LDH with Mg:Al ratio of 3 (Mg_3-Al/DBS) and 6 (Mg_6Al/DBS) in the 4-dodecylbenzenesulfonate (DBS) form were prepared by the co-precipitation method at a constant pH [20].

A solution (solution A) was prepared by dissolving $MgCl_2 \cdot 6H_2O$ and $AlCl_3 \cdot 6H_2O$ in 250 mL of water with a total Mg + Al concentration of 1 mol/L and a ratio Mg:Al of 3 or 6. A second solution (solution B) was prepared dissolving NaOH in 600 mL of water (NaOH concentration 1 mol/L).

A third solution (solution C) was prepared by dissolving 4-dodecylbenzenesulfonic acid (propanol solution 70% mass fraction) in 350 mL water; the quantity of DBS used was double the anionic exchange capacity of the LDH (i.e. DBS mol = 2Al mol). Solution C was neutralized directly in the 4-neck vessel used for the synthesis; NaOH was added until a pH = 10 was reached.

Solutions A and B were added drop-wise to solution C with intense stirring (35 rad/s), with a pH of 10.0 ± 0.2. Addition was completed in 4 h. The slurry was filtered without washing and dried in vacuo at 100 °C. The clay ($\approx$20 g) was aged for 17 h at 100 °C in refluxing conditions in 250 mL water containing a quantity of surfactant that is double the theoretical exchange capacity of the LDH. The excess of DBS surfactant was removed overnight by Soxhlet extraction with boiling water and, finally, the modified anionic clay was dried again in vacuo at 100 °C for 8 h. The neutralization, aging, Soxhlet extraction as well as all the synthesis were conducted in an argon atmosphere to minimize carbonate contamination.

2.2. Preparation of LDH/PA6 nanocomposites

Materials were preconditioned as follows: PA6 was dried in vacuo at 80 °C for 2 h and stored in vacuo overnight. The LDH were dried overnight in a desiccator in vacuo. The LDH (0.2 g) were dispersed in 3.8 g PA6 (5% mass fraction LDH content) using a twin-screw, co-rotating micro-extruder (DACA Instruments). Different temperature and shear stress processing conditions were investigated, but the residence time in the extruder was held constant at 15 min.

2.3. Characterizations and measurements

Extruded LDH/PA6 samples were hot pressed at 240 °C and slowly cooled (5–10) °C/min in air in a 20 mm × 13 mm × 2 mm plate shape for WAXD and SAXS. Quenched samples were prepared reheating the samples up to 280 °C for 5 min and cooling to room temperature at a rate of 50 °C/min. Wide-angle X-ray scattering (WAXD) was performed with a Philips electronic instruments XRG 3100 using Cu Kα1 radiation (λ = 0.154059 nm) and step size of 0.04°. The *d*-spacing uncertainty was 0.01 nm (2σ) as determined by running a modified LDH (Mg_3Al/DBS) three times. For peak fitting analysis, the multipeak fitting package included with IGOR Pro version 5.04b2 from Wavemetrics, Inc., was used. A Voigt peak shape was found to provide the best fit to the data, by including instrumental broadening artifacts found in the data. Peaks were added to the fit for the (200), (202), and (002) characteristic reflections of polyamide 6 alpha phase, as well as for the (200) reflection of the gamma phase and for scattering from amorphous material (the amorphous halo) [41–43]. As in the cited references, for this analysis the polymer chain lies in the *b*-axis direction of the monoclinic unit cell, in contrast to standard analysis of polymer crystal structures.

Small-angle X-ray scattering (SAXS) data were collected using a Bruker Hi-Star 2D area detector, with X-rays produced by a Rigaku Ultrax18 rotating anode X-ray generator operated at 40 kV and 60 mA. The Cu radiation was monochromated with pyrolytic graphite, giving a resultant wavelength of λ = 0.15418 nm. The sample-to-detector distance was approximately 65 cm. The raw data were azimuthally averaged and then corrected for detector noise and background radiation. The corrected data are presented as intensity as a function of the magnitude of the scattering vector, q, where $q = 4\pi \sin(\theta)/\lambda$, where 2θ is the scattering angle. The real-space length scale, d, is given as $d = 2\pi/q$.

The carbon, hydrogen, sulfur, aluminum, magnesium, chlorine and water content of the LDH were determined by Galbraith Laboratories, Inc. (Knoxville, USA). A Philips 400T electron microscope was used to obtain bright-field TEM images at 120 kV under low-dose conditions. Micrographs of LDH only were achieved by dispersing LDH in isopropanol by ultrasonication and transferring a small drop of the suspension to a carbon coated grid. Polymer nanocomposite samples were ultramicrotomed at −60 °C using a diamond knife on a Leica Ultracut UCT microtome to give 70 nm thick sections. The thermogravimetric analysis (TGA) was performed on a Hi Res TGA 2950 TA instrument with platinum pans; the size of the samples was about 10 mg, the heating rate 10 °C/min and the atmosphere nitrogen (flowing rate 50 cm^3/min). The peak mass loss rate had an uncertainty of 1.5 °C (2σ). The differential scanning calorimetry (DSC) was recorded using a TA Instruments DSC2910 at a heating/cooling rate of 2 °C/min; the nitrogen flow rate was 50 cm^3/min and the sample size around 8 mg. The peak heat flow had an uncertainty of 0.8 °C. SymApps software (Bio-Rad Laboratories), with a molecular mechanics based on the MM2 force field, was used to estimate the Van der Waals dimensions of intercalated species.

3. Results and discussion

The development of a method for the preparation of an organo-modified LDH, appropriate to melt processing, required considerable experimentation for the selection of the best synthesis conditions. Dodecylbenzenesolfonate anion (DBS) was used as organic compatibilizer to achieve an organophilic media in the LDH inter-layer region. DBS was preferred to other possible surfactants such as dodecylsulfate, stearic acid and phosphorus based anionic surfactants, due to its excellent combination of high thermal stability, low cost and high water solubility. In particular the onset of thermal degradation for DBS is 430 °C (not shown) and it is comparable to the one observed for imidazolium salts [44]. Imidazolium salts are the most thermally stable compatibilizers known for cationic clays but they are extremely expensive.

Table 1
Composition of synthesized LDH

	Mg_3Al/DBS (%w)	Mg_6Al/DBS (%w)
Element		
Mg	10.61±0.69	12.10±0.79
Al	3.88±0.25	2.65±0.17
C	37.01±0.28	37.49±0.28
H	7.01±0.40	6.93±0.40
N	<0.5	<0.5
S	4.90±0.72	4.61±0.67
Cl	$(4.5\pm1.0)\times10^{-3}$	$(4.2\pm0.9)\times10^{-3}$
H_2O	5.38±0.15	5.46±0.15
Mole ratio (mole/mole)		
Mg:Al	3.03±0.25	5.07±0.42
S:Al	1.06±0.20	1.46±0.28

Reported uncertainty is $\pm2\sigma$ where σ is the standard deviation. The uncertainty of calculated ratios Mg:Al and S:Al is obtained combining individual standard uncertainties according to the law of propagation of uncertainty.

The availability of high performance and low cost surfactant, such as DBS, will likely increase in the future the interest for anionic clays versus cationic clays based nanocomposites.

In a previous paper [21], the possibility of synthesizing magnesium–aluminium LDH in the 4-dodecylbenzenesulfonate form (Mg–Al/DBS) was explored, but the crystallinity was poor and/or the exchange was incomplete even though the authors explored three different methods of synthesis (reconstruction, exchange and co-precipitation). Furthermore, the AEC was high (Mg/Al = 3). In the current work, it was found that synthesis of Mg–Al/DBS LDH with a low AEC and without MgO impurities (as detected by WAXD), required that the maximum Mg/Al ratio between the reagents be no more than 6. The actual ratio in LDH is 5.1 (Table 1). When a Mg/Al ratio of 7 was used, WAXD reveled the presence of MgO (not shown). It is noteworthy that alternate methods to the co-precipitation in presence of the organic anion, such as anionic exchange of a Mg/Al LDH in a chloride form, appear to be unsuccessful in completing the exchange, giving rise to a mixture of an intercalated phase and pristine inorganic phase.

In Fig. 1, WAXD patterns for the two organo-modified LDH prepared by co-precipitation are displayed. LDH layers may exhibit two stacking sequences, rhombohedral and hexagonal [20]. The hexagonal symmetry is possibly obtained at high temperatures synthesis conditions, but it is rare. Due to the broadness of WAXD peaks shown in Fig. 1, the actual symmetry of the organo-modified LDH cannot be proved. However, for convenience LDH diffraction patterns are indexed according to the common rhombohedral symmetry (space group *R*-3*m*). The unit cell parameters are *a*—which is the distance between two adjacent cations (M and M^{III}), and $c' = 3c$—where *c* is the basal distance between two stacked layers. A unit cell in the *R*-3*m* symmetry is formed by three stacked octahedral sheets and, therefore, the distance *c* between two stacked lamellae is indexed as d_{003} diffraction peak. WAXD patterns show three orders of diffraction (003), (006), (009), indicating that the layer structure is well ordered. The observed *d*-spacing (as it will be discussed below) suggests

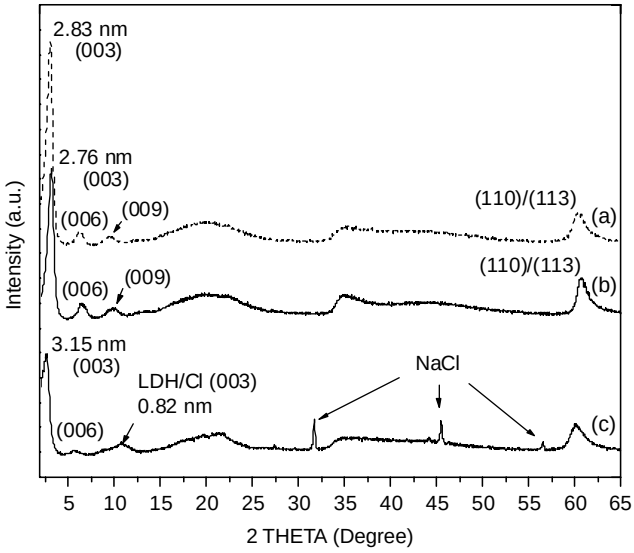

Fig. 1. Powder diffraction patterns (WAXD) for: (a) Mg_6Al/DBS; (b) Mg_3Al/DBS after Soxhlet extraction with water; and (c) Mg_6Al/DBS after Soxhlet extraction with ethanol.

a monolayer arrangement of DBS. Both Mg_3Al/DBS and Mg_6Al/DBS patterns show a hump at about 20°. It could be argued that this is related to the presence of a small amount of amorphous MgO. However, even if MgO segregation might be likely for LDH with high Mg content such as Mg_6Al/DBS, it is not the case for Mg_3Al/DBS; furthermore an increase in the amorphous MgO phase (i.e. an increase in the intensity of the hump) and/or the formation of crystalline MgO (i.e. appearance of WAXD peaks associated with MgO) should be observed in the Mg_6Al/DBS LDH compared to Mg_3Al/DBS LDH. As shown in Fig. 1 this is not the case. A similar broad scattering hump in the same 2θ range is observed when DBS acid is neutralized with NaOH (not shown) and, in a previous paper [45], a similar hump was attributed to the presence of adsorbed poly(ethylene glycol)alkenylsulfonic acid on the surface of LDH. The broad peak in Fig. 1, therefore, can be assigned to the presence of the organic surfactant.

The TEM micrograph of Mg_6Al/DBS (Fig. 2) shows the typical hexagonal platy structure of LDH on the edge of an agglomerate. The planar plate size is in between 70 and 200 nm.

The small amount of chloride detected by elemental analysis (Table 1) indicates that chloride coming from reagents ($MgCl_2\cdot6H_2O$ and $AlCl_3\cdot6H_2O$) is removed during aging and Soxhlet extraction with water, and that the intercalated chloride anions are negligible compared to sulfonate anions (Cl:S mole ratio is about 8×10^{-4} for both Mg_3Al/DBS and Mg_6Al/DBS).

When ethanol was used instead of water for the Soxhlet extraction the final product was a mixed LDH in which Cl and DBS anions coexisted (Fig. 1(c)), and as pointed out by the three sharp peaks detected by WAXD (d = 0.182, 0.199, 0.163 nm), NaCl could not be completely removed. Soxhlet extraction acts also as a hydrothermal treatment and water extraction, compared to ethanol, guarantees a higher

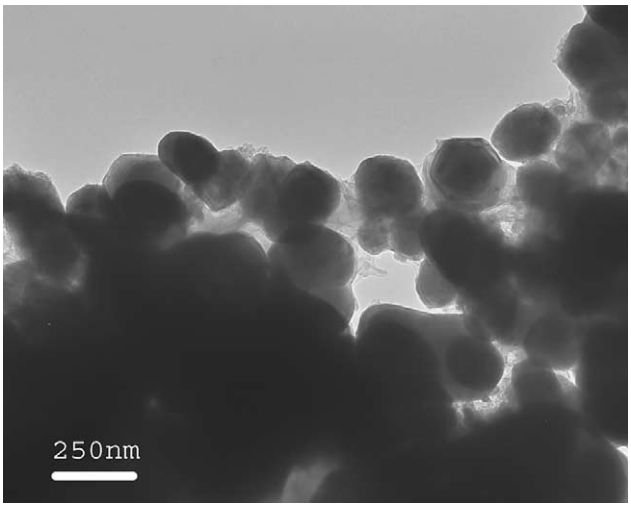

Fig. 2. TEM micrograph of Mg_6Al/DBS.

crystallinity LDH as evidenced by the intensity and sharpness of the (003) reflections in Fig. 3 [46,47].

The elemental analysis shows that there is a good agreement between the actual and the theoretical Mg:Al ratio (ρ_{act} and ρ_{theor}, respectively) for Mg_3Al/DBS; this is not the case for Mg_6Al/DBS ($\rho_{act}=5.07$, $\rho_{theor}=6$). Similar results were observed in previous experiments [39]. Computational studies demonstrated that the formation energy as a function of ρ shows a minimum at $\rho=3$, and even if Mg:Al ratio can be freely changed during the synthesis, the highest actual value of ρ achievable (ρ_{max}) is limited [48].

The value of the lattice parameter a is usually calculated from the WAXD diffraction peak d_{110} as $a=2d_{110}$. However, for organic modified LDH the low intensity and the overlapping of d_{110} and d_{113} peaks may not allow an exact measure of a (Fig. 1). It is reported that the unit cell a depends on the size of the cations M and M^{3+}, decreases linearly as the M^{3+} content increases, and is independent of the type of intercalated anion [49–51]. For this reason a can be estimated on the basis of the Mg:Al ratio and the available data from literature [18]. The determined values of a with this approach are 0.306 and 0.311 nm for $\rho=3$ and 5, respectively. The parameter a is necessary for the calculation of the layer charge density (σ) which generates the electrostatic attractive forces between the lamellae. σ is determined as the ratio between the layer charge x and the area of an octahedral unit, and can be expressed as $\sigma=2x/(a^2\sqrt{3})$. The corresponding values of σ are 3.09 charge/nm^2 for Mg_3Al/DBS, and 1.91 charge/nm^2 for Mg_6Al/DBS. Supposing that half of the positive charges in LDH lamellae are neutralized from each side of the layer, the corresponding values of available area per monovalent anion Σ (where $\Sigma=2\sigma^{-1}$) are 0.64 and 1.04 nm^2/charge for Mg_3Al/DBS and Mg_6Al/DBS, respectively. It implies that the surfactant layer density in Mg_3Al/DBS is considerably higher compared to Mg_6Al/DBS.

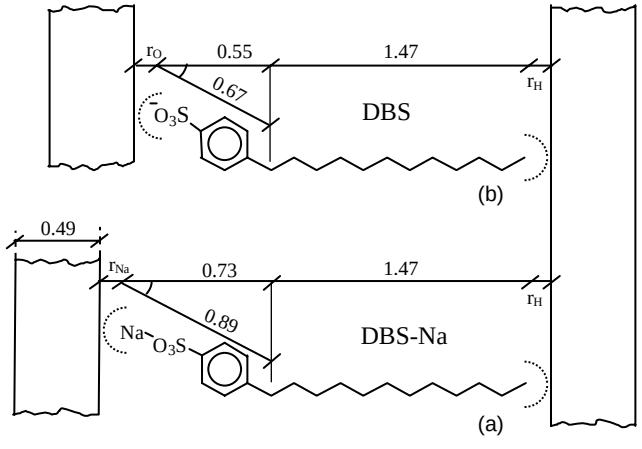

Fig. 3. Interlamellar arrangement in LDH of: (a) dodecylbenzenesulfonate sodium salt (calculated d-spacing 2.99 nm); (b) dodecylbenzenesulfonate anion (calculated d-spacing 2.76 nm). r_O, r_H, r_{Na} are the van der Waals radii of O, H and Na, respectively.

Elemental analysis indicates that for a Mg:Al ratio of 6 there are more sulfonate groups than expected. In fact for the electrical neutrality of the crystal it is necessary that there is one intercalated monovalent anion for each Al atom. Instead, as reported in Table 1, S:Al ratio is 1.46, thus in Mg_6Al/DBS there are 1.46 sulfonate groups for each Al atom. This large excess is related to the intercalation of neutral sodium dodecylbenzenesulfonate (DBS-Na) due to the high affinity of this salt for LDH surfaces [21]. Instead no excess of surfactant is observed for the sample Mg_3Al/DBS. In a monolayer arrangement each DBS anion occupies an area on the LDH surface equal to ~0.5 nm^2. This value is calculated as the sum of the cross-sectional area of the anionic head (~0.3 nm^2)[6] and the aliphatic chain (0.2 nm^2) [52]. The available area per monovalent anion Σ is lower for the Mg:Al=3 ($\Sigma=0.64$ nm^2/charge), than for Mg:Al=6 ($\Sigma=1.04$ nm^2/charge).The small difference between the calculated cross-sectional area of DBS and the available area per anion justifies the lack of intercalated DBS-Na in Mg_3Al/DBS, whereas in Mg_6Al/DBS the free space between the layers—that is not taken up by DBS anions necessary to guarantee electrical neutrality—can be filled by DBS-Na intercalated molecules.

In Fig. 3, the proposed scheme suggests a monolayer all-trans arrangement of surfactant anions and salts in the inter-layer region of the synthesized LDH. It is supposed that the alkyl chain of dodecylbenzenesulfonate anions is oriented perpendicular to the layer and that the benzene ring is tilted at a θ angle of 35°. The d-spacing can be calculated as follows:

$$d_{calculated} = d_{layer} + d_{inter}$$

where $d_{layer}=0.49$ nm is the thickness of brucite-type layer [16] and d_{inter} is the van der Waals length of the intercalated species. The dimensions of DBS-Na salt and DBS anion reported in Fig. 3 are estimated by computer modeling supposing an all-trans configuration and van der Waals radii of 0.11 nm for H, 0.19 nm for Na and 0.14 nm for O. The calculated d-spacings are 2.76 and 2.99 nm for DBS and DBS-Na, respectively. In Mg_3Al/DBS only DBS is present in the inter-layer region and the observed d-spacing (2.76 nm) is in

[6] Cross-sectional area calculated by means of computer modeling.

Table 2
Formulas and characteristic parameters of synthesized LDH

LDH	Nominal formula for octahedral unit	c (nm)	a[a] (nm)	σ (charge/nm^2)	AEC[b] (mequiv./100 g)
Mg_3Al/DBS	$Mg_{0.75}Al_{0.25}(OH)_{2.00}(C_{18}H_{29}SO_3)_{0.25}\cdot 0.44H_2O$	2.76	0.306	3.09	169
Mg_6Al/DBS	$Mg_{0.84}Al_{0.16}(OH)_{2.00}(C_{18}H_{29}SO_3)_{0.16}\cdot (C_{18}H_{29}SO_3Na)_{0.08}\cdot 0.44H_2O$	2.83	0.311	1.91	109

[a] Value estimated by the Mg:Al ratio (see text).
[b] The AEC is calculated as follow: $AEC = x/M_w \times 10^5$ (mequiv./100 g) where M_w is the weight of the LDH nominal formula for octahedral unit.

agreement with the calculated one shown in Fig. 3(b). Instead in Mg_6Al/DBS there is both DBS and DBS-Na intercalated and the actual interlamellar arrangement is a combination of the two schematic ones shown in Fig. 3. Because LDH layers are less rigid than montmorillonite [53] and they bend in the transverse direction around the gallery anion [54], the observed value of d-spacing (2.83 nm) is a weighed average of the local spacings in the vicinity of the intercalated species. Supposing that the excess of S from elemental analysis is due to DBS-Na, then it follows that the ratio DBS:DBS-Na is 1:0.46, and the weighed average d-spacing is 2.83 nm (i.e. the same observed spacing in Fig. 1(a)). The perfect correspondence between theoretical and experimental data supports an all-trans configuration of surfactant alkyl tails.

The nominal formulas for an octahedral unit of synthesized LDH are found out on the basis of previous hypothesis and elemental analysis data, and are reported in Table 2 together with their pertinent characteristic parameters.

The thermogravimetrical analysis (Fig. 4) shows that the synthesized LDH exhibit a good thermal stability and can be utilized for melt processing of polyamide 6 as long as they are pre-dried at a temperature higher than 100 °C prior to processing.

Several samples were prepared by extruding polyamide 6 with Mg_6Al/DBS and Mg_3Al/DBS. The different processing conditions used are reported in Table 3. The lowest (230 °C) and the highest temperatures (260 °C) were chosen taking into account the melting temperature of PA6 and the thermal stability of organo-modified LDH, respectively. Intermediate temperatures were selected to show the influence of temperature and shear on the degree of exfoliation. WAXD diffraction patterns (Fig. 5) for Mg_6Al-235 (a) and Mg_6Al-230 (c) suggest a disordered nanocomposite (possibly delaminated) structure. The presence of a shoulder, or a wide peak, for the other samples (b, d, e and f) indicates a mixed micro/nano-composite morphology. This may indicate, in these cases, that only a fraction of LDH is intercalated (or exfoliated) to such an extent that 003 diffraction peak is no longer detectable by WAXD. The level of dispersion improves in all the samples by increasing the torque during extrusion (Table 3 and Fig. 5). It is also interesting to note that the shear increased when the processing temperature was decreased from 260 to 235 °C, where the best dispersion was achieved, while it decreased when the temperature was further decreased to 230 °C. This suggests that the degree of delamination, together with the temperature, plays an important role in rheological behaviour of the nanocomposite.

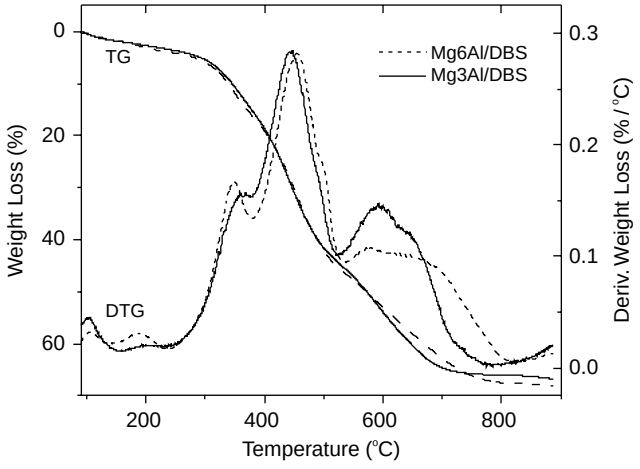

Fig. 4. Thermogravimetrical analyses of organic-modified LDH.

The results observed in this work are different from the ones previously reported for PA6 layered silicates nanocomposites. Dennis et al. [55] showed that the highest shear intensity configuration during melt compounding did not give the best dispersion. It could be argued that high shear could prevent a good dispersion due to the possible thermal degradation of the clay surfactant. Fornes et al. [56] pointed out that in PA6 surfactant degradation can even improve the exfoliation by increasing polar interactions between the polyamide chains and the clay. Therefore, while shear, together with the exchange capacity, seems to be the main factor for LDH dispersion in PA, shear is not the key to delamination in PA layered silicates nanocomposites. It is believed that hydrogen-bonding between

Table 3
Composition and processing conditions of extruded samples

Sample ID	Composition	Extrusion conditions		
		Temp. (°C)	Max torque (N m)	Rotat speed (rad/s)
PA6e	PA6	235	3.1	30.0
Mg6Al-235	PA6+5% Mg6Al/DBS	235	4.4	28.5
Mg3Al-235	PA6+5% Mg3Al/DBS	235	4.2	29.5
Mg6Al-230	PA6+5% Mg6Al/DBS	230	4.3	28.0
Mg6Al-240	PA6+5% Mg6Al/DBS	240	4.0	25.0
Mg6Al-245	PA6+5% Mg6Al/DBS	245	3.6	29.8
Mg6Al-260	PA6+5% Mg6Al/DBS	260	2.7	25.0

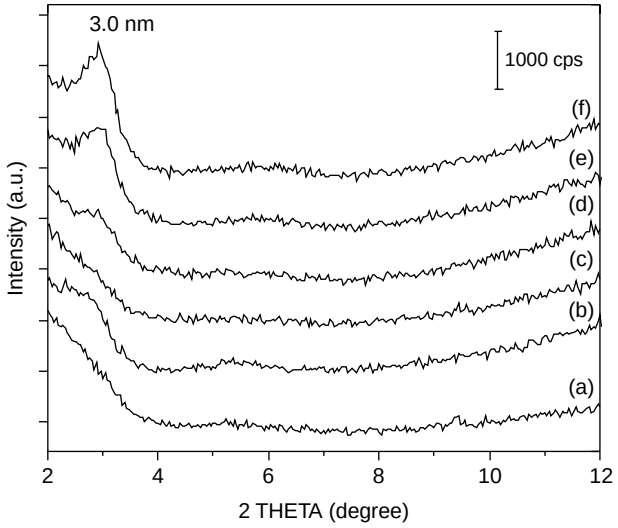

Fig. 5. WAXD data for: (a) Mg6Al-235 (4.4 N m), (b) Mg3Al-235 (4.2 N m), (c) Mg6Al-230 (4.3 N m), (d) Mg6Al-240 (4.0 N m), (e) Mg6Al-245 (3.6 N m), (f) Mg6Al-260 (2.7 N m).

clay and polyamide provides the driving force for polymer intercalation and aids subsequent exfoliation. This agrees with the lattice model of Vaia and Giannelis [57].

The TEM picture of Mg6Al-235 (Fig. 6) shows that, after extrusion, LDH layers loose their pristine stacked structure and form a homogenous exfoliated arrangement in the polymer matrix. In previous works even if a delaminated LDH structure was claimed, single layers could not be observed [38,59] and TEM pictures showed a non-homogenous agglomerated structure [35,58] or an ordered assembling of parallel aligned lamellae [33,34].

The planar plate size of Mg_6Al/DBS observed in the final nanocomposite (Fig. 6) is about (40–80) nm. This value is considerably lower then the one (70–200 nm) observed for the same clay before extrusion (vide supra). Therefore, during melt compounding, layer breakage occurs. A similar behavior was reported for montmorillonite [60] and it was related to the fragile nature of the clay. Even if LDH are less rigid then montmorillonite [53], a fragile fracture is the most likely explanation for the plate size reduction observed in Mg6Al-235. However, a layer's breakage related to a partial dehydroxylation of LDH cannot be excluded. In fact, even if the processing temperature used during compounding is 235 °C and the onset for the interlayer thermal degradation is 290 °C (Fig. 5), shear during compounding can produce local overheating.

It is interesting to note that, while the extrusion conditions for Mg6Al-235 a0nd Mg3Al-235 are the same, the shoulder in Mg3Al-235 (Fig. 5) suggests the presence of residual tactoids. This is confirmed by TEM picture of Mg3Al-235 (Fig. 7) in which 120–180 nm long tactoids are observed. The different behavior can be explained both by higher electrostatic attractive interactions [15,27,28] and higher surfactant layer density that can limit polymer-LDH favorable interactions in Mg_3Al/DBS compared to Mg_6Al/DBS. Balazs et al. [61] in their modeling based on the self-consistent field theory found out that the decrease of the surfactant layer density, to such an extent, enhances the dispersion and facilitate the polymer penetration and intermixing. These theoretical outcomes were experimentally confirmed by Fornes et al. [62] in PA6-montmorillonite nanocomposites.

The same principles can be applied for LDH. Due to the presence of DBS-Na intercalated in Mg_6Al/DBS, the actual density of the surfactant layer increases and the area available for each DBS anion or DBS-Na salt is 0.71 nm^2. This value is close to the value calculated for Mg_3Al/DBS (0.64 nm^2) and then the extent of interactions polymer–LDH is comparable. However, it is reasonable to think that at least a partial migration of the intercalated DBS-Na salt occurs during melt

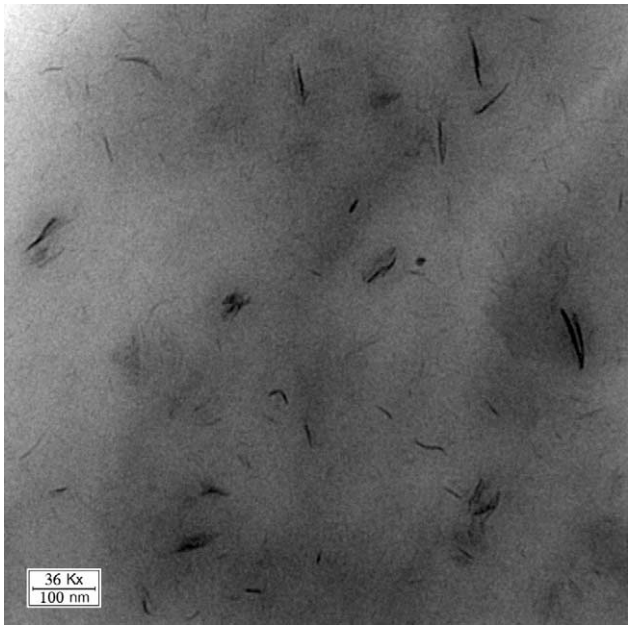

Fig. 6. TEM micrograph of Mg6Al-235.

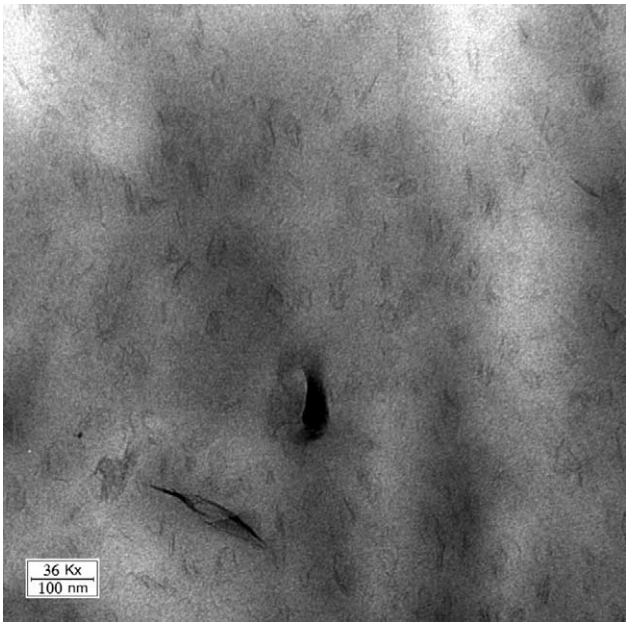

Fig. 7. TEM micrograph of Mg3Al-235.

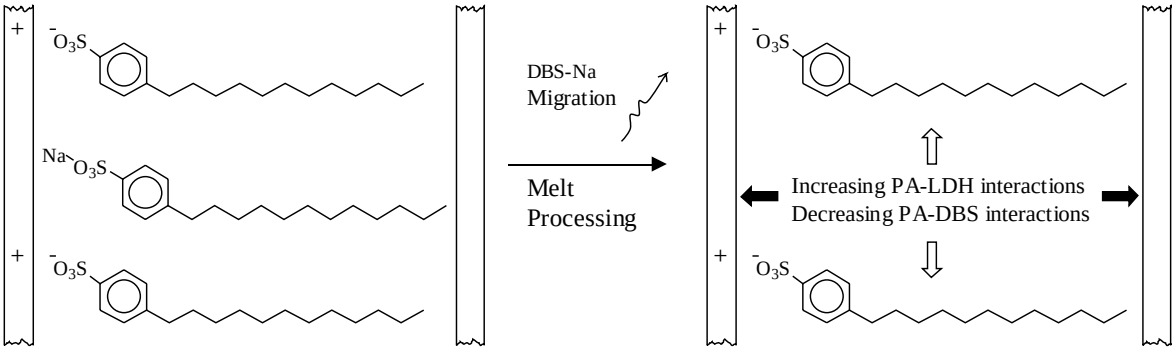

Fig. 8. Migration of DBS-Na salt intercalated in Mg_6Al/DBS during melting compound.

compounding. In this way the unfavorable surfactant-PA6 interactions are decreased whereas favorable polar interactions and hydrogen bondings between PA6 and LDH are increased, as depicted in Fig. 8.

The high degree of exfoliation in Mg_6Al/DBS is also supported by small-angle X-ray scattering (SAXS) data. In Fig. 9, the SAXS patterns of extruded polyamide 6 (PA6e), and nanocomposite Mg_6Al-235 are shown. The processing conditions for the two samples during extrusion were the same, as reported in Table 3. For the LDH-based nanocomposite, a weak reflection is observed around $q=2\ nm^{-1}$. The absence of a strong reflection at this angle is indicative of an intercalated or delaminated structure, but the presence of the weak reflection also suggests that a small number of LDH layers which are still stacked remain. These layers retain their pristine basal distance, or are slightly intercalated by polymer. This observation is consistent with the TEM data, in which imaging limitations often result in multilayered tactoids appearing as single layers and in which only a miniscule sample volume is illuminated. Thus, the combination of the SAXS and TEM data indicate that the LDH materials are very highly exfoliated in the Mg6Al-235 nanocomposite, and that a small fraction of unexfoliated material is present.

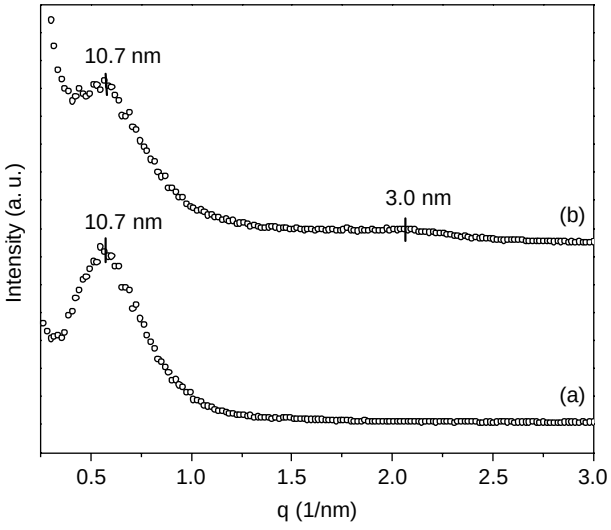

Fig. 9. Small angle X-ray scattering (SAXS) patterns for: (a) PA6e; (b) Mg6Al-235.

The marked peak at $q=0.59\ nm^{-1}$ in the SAXS profile for PA6e (Fig. 9(a)) shows the presence of lamellar crystallites with a periodic d-spacing of 10.7 nm. In presence of LDH, the same peak is less pronounced as observed for Mg_6Al-235. Similar results have been reported for polyamide 6 nanocomposites based on layered silicate [63,64]: the authors speculate that clay layers disrupt the lamellar superstructure by spatial arrangement of the clay. In this work the intensities of the peaks at $d=10.7$ nm (Fig. 9) for the neat polymer and the LDH nanocomposite are approximately the same, but the presence of LDH is increasing the scattering at very low angles (i.e. $q<0.5\ nm^{-1}$). Therefore, it is quite likely that the polymer lamellar superstructure is unaffected by the presence of LDH.

In spite of the characteristic barrier effect of layered nanocomposites [65] the thermogravimetrical analysis (Fig. 10) shows a reduction of about 37 °C in the peak of derivative weight for Mg6Al-235 as compared to the neat PA6e. Similarly, a decrease in the thermal stability of the nanocomposite is pointed out by a reduction of about 30 °C in the onset of thermal decomposition temperature. This is in contrast with the results previously obtained for other LDH based nanocomposites [33,34,36]. A nucleophilic attack mechanism is a possible explanation for the reduction in the thermal stability. In fact, Davis et al. [66] reported that, in the presence of a nucleophile such as water or ammonium polyphosphate, the decomposition thermodynamics of PA6

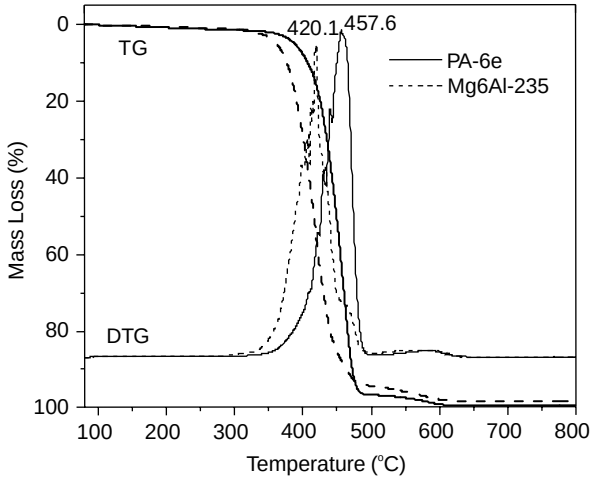

Fig. 10. TGA curves for PA6e and Mg6Al-235.

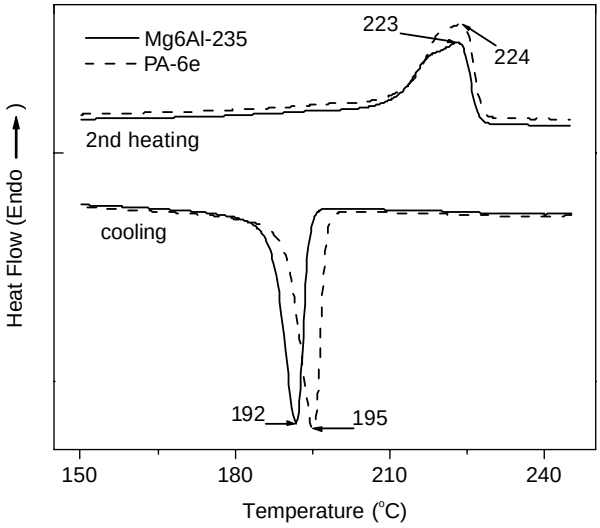

Fig. 11. DSC curves for PA6e and Mg6Al-235 at a cooling-heating rate of 2 °C/min (data collected during the second consecutive scan).

are altered and peptide scission near 300 °C results in a drastic decrease in polymer molecular mass and an increase in polymer end-groups content. The release of intercalated water or the partial dehydroxylation during melt compounding is a possible source of nucleophile. A nucleophilic attack mechanism can also be activated by DBS anions of Mg_6Al/DBS. In fact, like ammonium polyphosphate, sulfonate when heated decomposes to form strong mineral acids [67]. Therefore, it is reasonable that DBS can alter the pathway of PA6 decomposition like ammonium polyphosphate [68].

Silicate clays strongly influence the nature of the PA6 crystallization, favoring the formation of γ-phase crystals in addition to the α-form crystals observed in the neat PA6 matrix [63,64]. Moreover, DSC cooling scans show that exfoliated layered silicates increase the crystallization rate, and have a strong heterogeneous nucleation effect.

Differential scanning calorimetry analysis (Fig. 11), however, shows no such a difference in the crystallization behavior of LDH nanocomposites (Mg6Al-235) compared to neat PA6 (PA6e). Similarly, WAXD data in Fig. 12 for PA6e and Mg6Al-235 both show the presence of the two characteristic polyamide peaks at $2\theta = 20.5$ and 24.2° due to the presence of α-phase. No γ-phase peak but only a small hump is detected at $2\theta = 21.5°$.

Wu et al. [69] showed that montmorillonite and saponite promote γ-phase formation only for high cooling rates. Therefore, it could be argued that the low cooling rate, used for the preparation of samples (5–10 °C/min) and DSC scans (2 °C/min), can depress the effects of the clay on crystallization. For these reasons the nanocomposite (Mg6Al-235) and pure Nylon (PA6e) were quenched by heating up to 280 °C for 5 min and then cooling at a rate of 50 °C/min. For the remainder of the paper, those samples will be identified as quenched. In this case DSC patterns (Fig. 13) show a small endothermic peak related to the melting of γ-phase for neat PA6 and LDH nanocomposites at 207 and 209 °C, respectively, but again, both of them mainly crystallize in the α-phase.

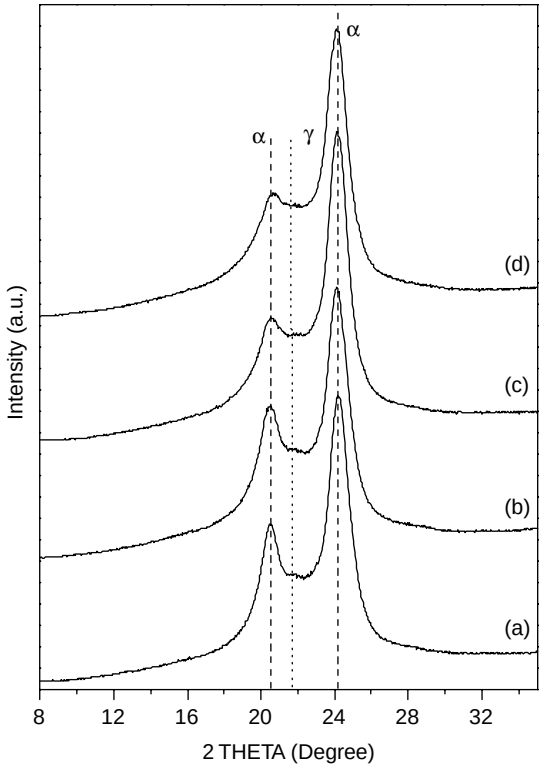

Fig. 12. X-ray data in the high 2-Theta range for: (a) PA6e; (b) Mg6Al-235; (c) PA6e quenched; (d) Mg6Al-235 quenched.

WAXD data of quenched samples are displayed in Fig. 14. Again, it is clear that there is only a minor amount of γ-phase present. Peak fitting allows a more careful check of the crystal structure. In the α crystal form, the two characteristic reflections correspond to the (200) reflection and a combination of the (202) and (002) reflections. Any γ-phase crystallinity will be indicated by the presence of the (200) reflection at $2\theta = 21.5°$ [63,64,69]. From the peak fitting analysis shown in Fig. 11 for the LDH-based nanocomposite sample, it is clear that there is only a minor amount of γ-phase present.

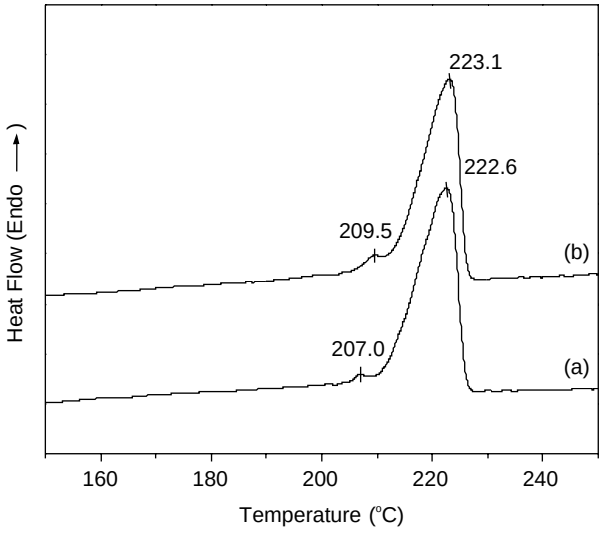

Fig. 13. DSC curves for (a) PA6e and (b) Mg6Al-235 after quenching.

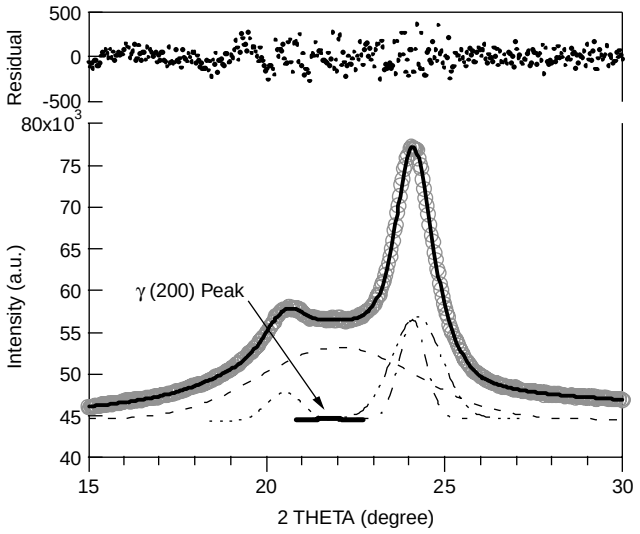

Fig. 14. WAXD data and peak fit analysis for the Mg6Al-235 LDH-based nanocomposite after annealing, showing a small peak corresponding to the γ-phase (200) reflection.

Table 4 lists the peak areas generated by the peak fitting analysis, and the relative percentage of gamma-phase as given by dividing the area of the gamma peak by the total area of the crystalline peaks in the range shown in Fig. 12. As shown in Table 4, the largest percentage of γ-phase is observed for the LDH-based nanocomposite after quenching, but that is only around 1.5% of the crystalline domains in the sample. The neat polyamide 6 appears to have only a trace of γ-phase after quenching, indicating that the LDH stabilizes very slightly the γ-phase, but at an extremely low level.

As a result, in this work neither a significant promotion in the γ-phase formation nor any change in the rate of crystallization was observed, suggesting that these effects are highly dependent upon the nature of the clay. Where the γ-phase becomes the dominant phase in layered silicate-based nanocomposites, in the current materials the dominance of the α-phase is consistent. This phenomenon is independent on the type of surfactant used [70] and is therefore explained by interaction between clay layers and PA6 molecules rather than by the effect of organic treatment. The available area per monovalent anion Σ is 1.04 nm^2/charge and 1.40 nm^2/charge for Mg_6Al/DBS and a medium value exchange capacity (108 mequiv./100 g) montmorillonite, respectively [71].

Table 4
Peak areas and resulting fraction of γ-phase from WAXS analysis

Peak		PA6e, before quenching	PA6e, after quenching	Mg6Al-235 before quenching	Mg6Al-235 after quenching
α-phase	(200)	17,200	9490	18,000	35,200
	(002)	34,600	21,800	27,500	27,400
γ-phase	(202)	11,200	29,400	17,700	27,700
	(200)	133	32	500	1300
Amorphous halo		64,800	29,400	27,700	5400
Fraction γ-phase		0.2%	0.1%	0.8%	1.5%

The value of Σ for Mg_6Al/DBS may be even lower if DBS-Na does not migrate completely during compounding. Considering the shielding effect of the surfactant, the available area for polymer–clay interactions is limited in LDH compared to montmorillonite. Therefore, it is reasonable to conclude that the low impact of LDH on the crystallization behavior is related to the low extent of interactions between PA6 and LDH surface.

4. Conclusions

Exfoliated LDH-based polyamide-6 nanocomposites can be prepared by melt processing when suitable organic-modified LDH with appropriate AEC values are synthesized. The presence of residue tactoids obtained with the high AEC LDH, and the almost complete exfoliation obtained with the low AEC LDH, suggest that electrostatic attractive forces and surfactant layer density between the layers may play an important role in the exfoliation mechanism. Shear, together with the exchange capacity, seems to be the key factor for the delamination of LDH in PA6. The decrease in LDH plate size in the nanocomposite reveals the breakage of clay layers during melt compounding, due to the fragility and/or the partial dehydroxylation of the LDH. A reduction in the onset of thermal decomposition temperature was observed in LDH/PA6 nanocomposites as compared to neat PA6e, which is most likely related to a nucleophilic attack mechanism. DSC and WAXD analyses suggest that no major change in the crystalline phase or in the rate of crystallization occurs with LDH nanocomposites. This is in contrast to the layered silicates/PA6 nanocomposites results, and suggests that these effects cannot be explained solely as a heterogeneous nucleation effect, but they are highly dependent upon the nature and extent of clay/polymer interactions.

References

[1] Alexandre M, Dubois P. Mater Sci Eng 2000;28(1):63.
[2] LeBaron PC, Wang Z, Pinnavaia TJ. Appl Clay Sci 1999;15:11–29.
[3] Okada A, Kawasumi M, Kurauchi T, Kamigaito O. Polym Prepr 1987; 28:447.
[4] Lan T, Pinnavaia TJ. Chem Mater 1994;6:573.
[5] Messersmith P, Giannelis EP. Chem Mater 1994;6:1719.
[6] Burnside SD, Giannelis EP. Chem Mater 1995;7:1597.
[7] Pinnavaia TJ. Science 1983;220:365.
[8] Gilman JW, Jackson CL, Morgan AB, Harris R, Manias E, Giannelis EP, et al. Chem Mater 2000;12:1866.
[9] Pinnavaia TJ. Science 1983;220:365.
[10] Okada A, Usuki A. Mater Sci Eng C: Biomimetic Mater Sens Syst 1995;3: 109.
[11] Giannelis EP. Adv Mater 1996;8:29.
[12] Lagaly G. Appl Clay Sci 1999;15:1.
[13] Vaia RA, Giannelis EP. MRS Bull 2001;26:394.
[14] Giannelis EP, Krishnamoorti R, Manias E. Polym Confined Environ 1999;138:107–47.
[15] Leroux F, Besse JP. Chem Mater 2001;13:3507–15.
[16] Meyn M, Beneke K, Lagaly G. Inorg Chem 1990;29:5201–7.
[17] Borja M, Dutta PK. J Phys Chem 1992;96:5434–44.
[18] Zhao Y, Li F, Zhang R, Evans DG, Duan X. Chem Mater 2002;14: 4286–91.

[19] Ogawa M, Kaiho H. Langmuir 2002;(18):4240–2.
[20] Vaccari A. Catal Today 1998;53–71.
[21] You Y, Zhao H, Vance GF. J Mater Chem 2002;12:907–12.
[22] Hibino T, Tsunashima A. Chem Mater 1998;10:4055.
[23] Yao K, Taniguchi M, Nakata M, Takahashi M, Yamagishi A. Langmuir 1998;14:2410–4.
[24] Ven L, Gemert MLM, Batenburg LF, Keern JJ, GielgensL H, Koster TPM, et al. Appl Clay Sci 2000;17:25–34.
[25] Kwak SY, Jeong YJ, Park JS, Choy JH. Solid State Ionics 2002;151: 229–34.
[26] Lan T, Kadiratna PD, Pinnavaia TJ. Chem Mater 1995;7:2144–50.
[27] Jacobson AJ. Mater Sci Forum 1994;152–153:1–12.
[28] Hibino T, Jones W. J Mater Chem 2001;11:1321–3.
[29] Hussein MZB, Yun-Hin TY, Tawang MM, Shahadan R. Mater Chem Phys 2002;74:265–71.
[30] Oriakhi OC, Farr IV, Lerner MM. Clays Clay Miner 1997;45:194–202.
[31] Oriakhi OC, Farr IV, Lerner MM. J Mater Chem 1996;6:103–7.
[32] Leroux F, Aranda P, Besse JP, Ruiz-Hitzky E. Eur J Inorg Chem 2003;1242–51.
[33] Hsueh HB, Chen CY. Polymer 2003;44:1151–61.
[34] Hsueh HB, Chen CY. Polymer 2003;44:5275–83.
[35] O'Leary S, O'Dermot D, Seeley G. Chem Commun 2002;1506–7.
[36] Chen W, Feng L, Qu B. Solid State Commun 2004;130:259–63.
[37] Bubniak GA, Schreiner WH, Mattoso N, Wypych F. Langmuir 2002;18: 5967–70.
[38] Chen W, Qu B. Chem Mater 2003;15:3208–13.
[39] Crepaldi EL, Pavan PC, Tronto J, Valim JB. J Colloid Interface Sci 2002; 248:429–42.
[40] Zammarano M, Franceschi M, Bellayer S, Gilman JW, Meriani S. Polymer 2005;46:9314–28.
[41] Tadokoro H. Structure of crystalline polymers. Malabar, FL: Robert E. Krieger Publishing; 1990.
[42] Holmes DR, Bunn CW, Smith DJ. J Polym Sci 1955;17:159–77.
[43] Arimoto H. J Polym Sci A 1964;2:2283–95.
[44] Wallid HA, Gilman JW, Nyden M, Harris RH, Sutto TE, Callahan J, et al. Thermochim Acta 2004;409:3–11.
[45] Leroux F, Aranda P, Besse JP, Ruiz-Hitzky E. Eur J Inorg Chem 2003; 1242:1251.
[46] Mohmel S, Kurzawski I, Uecker D, Muller D, Muller D, Gebner W. Cryst Res Technol 2002;37:4.
[47] Kannan S, Jasra RV. J Mater Chem 2000;10:2311–4.
[48] Trave A, Selloni A, Goursot A, Tichit D, Weber J. J Phys Chem 2002 B;106:12291–12296.
[49] Lopez-Salinas E, Garcia-Sanchez M, Montoya JA, Acosta DR, Abasolo JA, Schifter I. Langmuir 1997;13:4748–53.
[50] Parida K, Das J. J Mol Catal A: Chem 2000;151:185–92.
[51] Shaper H, Berg-Slot JJ, Stork WHJ. Appl Catal 1989;54:79–90.
[52] Hann RA. In: Roberts G, editor. Lagmuir–Blodget films. New York: Plenum; 1990. p. 17.
[53] Hines DR, Solin SA, Costantino U, Nocchetti M. Mol Cryst Liq Cryst 2000;341:1181.
[54] Gardner E, Huntoon KM, Pinnavaia TJ. Adv Mater 2001;13:1263.
[55] Dennis HR, Hunter DL, Chang D, Kim S, White S, White JL, et al. Polymer 2001;42:9513–22.
[56] Fornes TD, Yoon PJ, Paul DR. Polymer 2003;44:7545–56.
[57] Vaia RA, Giannellis EP. Macromolecules 1997;30:7990–8009.
[58] Costa FR, Abdel-Goad M, Wagenknecht U, Heinrech G. Polymer 2005; 46:4447–53.
[59] Adachi-Pagano M, Claude F, Besse JP. Chem Commun 2000;91–2.
[60] Yalcin B, Cakmak M. Polymer 2004;45:6623–38.
[61] Balazs AC, Singh C, Zhulina E, Lyatskaya Y. Acc Chem Res 1999;32: 651–7.
[62] Fornes TD, Hunter DL, Paul DR. Macromolecules 2004;(37):1793–8.
[63] Lincoln DM, Vaia RA, Wang ZG, Hsiao BS. Polymer;42(4):1621–1631.
[64] Lincoln DM, Vaia RA, Krishnamoorti R. Macromolecules 2004;37: 4554–61.
[65] Gilman JW, Kashiwagi T, Nyden M, Brown JET, Jackson CL, Lomakin S, et al. Chemistry and technology of polymer additives. Oxford, UK: Blackwell Science; 1999 [chapter 14].
[66] Davis DD, Gilman JW, Vander Hart DL. Polym Degrad Stab 2003;79: 111–21.
[67] Rhodes PR. 14th Annual BCC Conference on Flame Retardancy, June 2–4; 2003.
[68] Levchik SV, Costa L, Camino G. Polym Degrad Stab 1992;36:229.
[69] Wu T, Chen EC. Polym Eng Sci 2002;42:1141–50.
[70] Wu Q, Liu X, Berglund LA. Polymer 2002;43:2445–9.
[71] Aranda P, Ruiz-Hitzky E. Chem Mater 1992;4:1395.